Functional truncated membrane pores

SUPPORTING INFORMATION

APPENDIX

David Stoddart, Mariam Ayub, Lajos Höfler, Pinky Raychaudhuri, Jochen W. Klingelhoefer, Giovanni Maglia, Andrew Heron, Hagan Bayley

Department of Chemistry, University of Oxford, Oxford, OX1 3TA,

United Kingdom

Present addresses:

David Stoddart, Andrew Heron: Oxford Nanopore Technologies, Edmund Cartwright House, Oxford Science Park, Oxford OX4 4GA, United Kingdom

Jochen W. Klingelhoefer: LabMinds, 16 King Edward Street, OX1 4HT, United Kingdom

Giovanni Maglia: Department of Chemistry, University of Leuven, Leuven, 3001, Belgium

* Address: Department of Chemistry, University of Oxford, Oxford, OX1 3TA, United Kingdom. Phone: +44 1865 285101. Fax: +44 1865 275708. E-mail: hagan.bayley@chem.ox.ac.uk

Materials and Methods

1. Generation of truncated αHL genes

The αHL truncated barrel mutants (TBM) were generated from the NN gene in a pT7 vector (1, 2) by PCR mutagenesis and ligation-free in vivo recombination (3), and their sequences were verified. αHL NN/M113F/Δ120-125/Δ133-138 (TBMΔ6/M113F) was also prepared by PCR mutagenesis and ligation-free recombination by using the NN/Δ120-125/Δ133-138 gene (TBMΔ6) the in pT7 vector as a template.

2. Protein preparation

Heptameric αHL was produced as described in detail elsewhere (4). Briefly, an αHL polypeptide was expressed in the presence of [^{35}S]methionine in an E. coli in vitro transcription and translation (IVTT) system (E. coli T7 S30 Extract System for Circular DNA, Cat. #L1130, Promega) and incubated with rabbit red blood cell membranes for 1 h at 37°C to form heptamers (TBMΔ10 gave an assortment of products, Fig. 1*G*, main text). The membrane suspension was centrifuged at 25,000 X g and the pellet containing the heptamers was solubilized in loading buffer at room temperature and run on a 5% SDS-polyacrylamide gel overnight at 40 V. The gel was vacuum-dried for 3 to 4 h onto Whatman 3M filter paper, without heating. The dried gel was exposed to photographic film for 2 h and the developed film was used to locate the position of the heptameric protein in the gel. The protein-containing region of the gel was excised, rehydrated and crushed in 400 μL of 10 mM Tris.HCl, pH 8.0, containing 100 μM EDTA. The polyacrylamide was removed by centrifuging the suspension at 25,000 X g for 10 min at room temperature through a cellulose

micro spin column (Microfilterfuge tubes, Cat. #7016-024, Rainin). Aliquots of the purified protein were stored at -80°C.

3. Hemolysis Assays

αHL was made by IVTT in the absence of rabbit red blood cell membranes and the product was centrifuged at 25,000 X g. The hemolytic activity of the αHL in the supernatant was then assayed in microtiter wells. Typically 5 μL of the supernatant was diluted 20-fold in MBSA (10 mM 3-[N-morpholino]propane sulphonic acid (MOPS), 150 mM NaCl, pH 7.4, containing 1 mg mL^{-1} bovine serum albumin). This solution was subsequently serially two-fold diluted with MBSA such that each well contained a volume of 50 μL. An equal volume of washed rabbit red blood cells (~1% in MBSA) was then added to each well, starting with the well that contained the most diluted protein. Lysis was recorded by monitoring the decrease in light scattered at 595 nm with a microplate reader (Bio-Rad Laboratories Ltd, UK) (5).

4. Proteolysis of αHL proteins with proteinase K

Fresh proteinase K (Sigma Aldrich) solutions of 5.0, 0.5 and 0.05 mg mL^{-1} were prepared (from a 10 mg mL^{-1} stock) (5). αHL was prepared by IVTT in the absence of rabbit red blood cell membranes. The translation mix was centrifuged at 25,000 X g. 1 μL of the supernatant was diluted 40-fold with MBSA and pipetted into four tubes (9 μL in each). To three of the tubes, 1 μL of each of the different proteinase K solutions was added; 1 μL of water was added to the fourth tube, as a

control. After 5 min at room temperature, proteolysis was terminated by the addition of PMSF (phenylmethylsulfonyl fluoride) to 2 mM. Gel-loading buffer was added and the solutions were heated at 95°C for 5 min to denature oligomeric species. The products were analyzed by electrophoresis in 12% SDS-polyacrylamide gels (Bio-Rad Laboratories Ltd, UK. Cat # 345-0118)(5).

5. Native PAGE

Polyacrylamide gel electrophoresis in the absence of SDS was carried out with the NativePAGE™ gel system (Invitrogen Ltd, UK). ^{35}S-labeled proteins were prepared by IVTT and mixed with rabbit red blood cell membranes. After 1 h, the membrane suspension was centrifuged at 25,000 X g. The pellet was re-suspended in MBSA and solubilized in 2.5% DDM, before the addition of loading buffer. Unheated samples were subjected to electrophoresis in a 4-16% Bis-Tris NativePAGE™ gel (Invitrogen Ltd, UK. Cat # BN1002). The gel (containing Coomassie G-250) was then “fixed” by shaking in 40% ethanol/ 10% acetic acid in water for 1 h and destained overnight in 8% acetic acid. The gel was vacuum-dried for 1 to 2 h onto Whatman 3M filter paper, with heating at 90°C. The dried gel was exposed to photographic film for 3 h and the developed film was used to locate the position of the radio-labeled protein in the gel.

6. Planar bilayer recording

Electrical recordings were carried out with a planar lipid bilayer apparatus with bilayers of 1,2-diphytanoyl-sn-glycero-3-phosphocholine (DPhPC, Avanti Polar

Lipids), unless otherwise stated. Bilayers were formed (6) across an aperture (~100 μm in diameter) in a 25-μm thick polytetrafluoroethylene (Teflon) film (Goodfellow, Cambridge, Cat. #FP301200/10), which separated the apparatus into *cis* and *trans* compartments. The transmembrane potential is given as the potential on the *trans* side (i.e. the *trans* potential minus the *cis* potential, which was at ground). A positive current is one in which positive charge moves through the bilayer from the *trans* to *cis* side.

The aperture was first pre-treated with hexadecane in n-pentane (10 mg mL^{-1}). Electrolyte solution (0.5 mL: 1 M KCl, 25 mM Tris.HCl, 0.1 mM EDTA, pH 8.0) was added to both compartments. Then, DPhPC in n-pentane (5 μL, 10 mg mL^{-1}) was added to both sides. The pentane was allowed to evaporate and a bilayer was formed by lowering and raising the electrolyte level past the aperture. All current recordings were performed with a patch clamp amplifier (Axopatch 200B, Molecular Devices). αHL pores were added to the *cis* compartment.

To examine cyclodextrin (CD) binding, 80 μM of either βCD, γCD or $am_7βCD$ was added to the trans compartment, which was connected to the head-stage of the amplifier. Currents were typically recorded for 5 to 15 min at potentials between +100 to +200 mV. After the addition of a CD, transient current blockades were observed ($I_{RES\%}$ ~30%, SI Appendix-Figs. S4-S6). Mean τ_{on} (inter-event intervals) and τ_{off} (CD residence times) values were obtained for each αHL pore at various CD concentrations. The association and dissociation rate constants, k_{on} and k_{off}, were then determined from plots of $1/\tau_{on}$ and $1/\tau_{off}$ versus [CD] by using the linear fit tools in OriginPro8 (SI Appendix-Fig. S7). Dissociation constants ($K_D = k_{off}/k_{on}$) were

calculated from the rate constants and the errors (s.d.) in the K_D values propagated from the errors in k_{on} and k_{off} (Equation 1).

Equation 1.
$$Z = X / Y$$
$$\Delta Z = Z\sqrt{(\Delta X / X)^2 + (\Delta Y / Y)^2}$$

7. Droplet interface bilayers (DIBs) recordings

The single-chain F-amphiphile F_6FC and DPhPC were used to form asymmetric bilayers by using the "lipid-in" method of forming droplet interface bilayers (7, 8). DPhPC (25 mg, Avanti Polar Lipids, Alabaster, AL) was dissolved in pentane (2.5 mL) (Sigma Aldrich, Dorset, UK) and dried in a glass vial under a stream of nitrogen and then in a vacuum desiccator for 1 to 2 h. The lipid was rehydrated by vortexing with 1 M KCl, 10 mM Tris.HCl, pH 7.0, to give a final concentration of 10 mM. DPhPC liposomes were prepared by extrusion (Mini-Extruder, Avanti Polar Lipids, Alabaster, AL) of this lipid suspension through two 0.1 μm polycarbonate membrane filters. The extruded liposomes were stored at 4°C and diluted as required in 1 M KCl, 10 mM Tris.HCl, pH 7.0. Fluorinated fos-choline (100 mM, F_6FC, catalog no. F300F, Affymetrix, Santa Clara, CA) was stored at 4°C and diluted as required in 1 M KCl, 10 mM Tris.HCl, pH 7.0.

The chamber for electrical recording was filled with hexadecane (400 μL). Two Ag/AgCl wire electrodes were mounted on separate micromanipulators to enable independent positioning of the droplets. The tips of the Ag/AgCl electrodes were coated with 5% (w/v) low-melt agarose, which served as hydrophilic anchors from which droplets could be suspended. Typically, droplets (~250 nL) were deposited onto the electrodes careful extrusion from a pipet. For symmetric DPhPC

bilayers, a 1 mM DPhPC vesicle solution in 1 M KCl 10 mM Tris.HCl, pH 7.0, was hung on each electrode. For asymmetric DPhPC-F_6FC bilayers, a 1 mM DPhPC vesicle solution in 1 M KCl, 10 mM Tris.HCl, pH 7.0, was suspended from one electrode, and 1 mM F_6FC in 1 M KCl, 10 mM Tris.HCl, pH 7.0, was attached to the other. The droplets connected to the electrodes were allowed to incubate in the oil at room temperature until they had acquired well-ordered monolayers (30 min for DPhPC; >10 h for F_6FC). When two incubated droplets were brought together with the micromanipulator, bilayer formation occurred spontaneously and was observed electrically by measuring the capacitance by applying a triangular voltage wave. For current recording, the electrode carrying the droplet with the TBMΔ8 protein was connected to the ground of the patch-clamp headstage.

8. Molecular dynamics (MD) simulations

All-atom MD simulations were employed to generate the truncated barrel heptameric structures (main text, Fig. 1). First, structures of the truncated barrel mutants (TBM) heptamers were derived by homology modeling based on the WT αHL crystal structure (pdb: 7AHL) (9) by using the MODELLER suite (10). The TBMs were then inserted into a preformed 1, 2-dipalmitoyl-phosphatidylcholine (DPPC) bilayer (11) consisting of 512 lipid molecules. The system was then solvated with an electrolyte bath consisting of SPC water molecules and potassium and chloride ions. After initial energy minimization to relax steric conflicts by using the steepest descent method in GROMACS(12), molecular dynamics were simulated for 10 ns. The configurations of the TBMs (main text, Fig. 1) were taken from the final snapshot.

The MD run was performed by using GROMACS at an atomistic level of detail, employing the GROMOS96 53a6 field to represent inter- and intra-molecular long- and short-range interactions. Full periodic boundary conditions were applied to the system. The time-step for integration was 2 fs and simulation frames were stored every 5 ps for subsequent analysis. The non-bonded neighbor list was updated every ten steps. Atomic charges were assigned on the basis of the default atomic charge values specified in the GROMOS96 53a6 force field. The Van der Waals interactions were modeled using a cut-off distance of 12.0 Å. In the simulation, the cell temperature was maintained at 323 K with the Berendsen temperature-coupling algorithm. The Berendsen pressure-coupling algorithm was applied to maintain the pressure at 1.0 bar (13).

For long simulations (>μs), we employed coarse-grained molecular dynamics. Coarse graining allowed us to extend the range of the simulations in both space and time compared to all-atom models. In the Marrink coarse-grained (CG) force field (14), an all-atom system is converted to a CG representation by putting clusters of atoms with similar physical properties into one CG grain (bead). These grains contain four or five atoms (excluding hydrogen). Bead classes are based on properties such as polarity, hydrogen bonding, or charge, which are used to determine the strength of non-bonded interactions between any two grains in the system. Standard masses, bond lengths and force constraints were used for all of the bonded interactions in the system to further improve the speed of the simulation (14).

A truncated barrel mutant (TBM) of α-hemolysin was placed in a simulation box of 18 x 18 x 18 nm initial dimensions. Position restraints were applied to the

backbone of the TBM. The protein was inserted in an equilibrated 90% DPPC/ 10% DLPC bilayer. DPPC was substituted for DPhPC because a coarse-grained (CG) representation of DPPC is available. The CG approach is undoubtedly an approximation. Indeed, DPPC and DPhPC can be represented by the same structure, since 4 to 5 heavy atoms are typically grouped in a single grain. The one extra atom due to methyl groups in eight of the grains in DPhPC does not change the classification of these grains, which is C1 in the MARTINI CG force-field (14).

An initial thinning of the lipid bilayer occurred after the following steps. The lipid molecules that would occupy the same space as the TBM were removed. The remaining lipid molecules were normal to the plane of the bilayer at this point. The lipid-TBM system was then solvated in water. The water molecules that ended up in the bilayer were removed. Potassium and chloride ions were added to give a concentration of 0.5 M. Seven additional chloride ions were added as counterions to neutralize the positive charge on the protein. The final system included approximately 60,000 beads. Steepest decent energy minimization was run on the system. Four ns of preconditioning MD were run with a constant number of particles and at a constant volume. In this step, the temperature of the system was brought to 300 K. After this MD step, the lipid molecules adopted a half-toroidal structure near the *trans* opening of the TBM (SI Appendix-Fig. S8, t = 0 ns), with lipid headgroups lining the bottom part of the conductive pathway. The configuration at the end of this 4 ns run was the initial configuration (0 ns) for the actual MD run. In the actual MD run, the number of particles, the pressure, and the temperature (300 K) were constant.

CG simulations were performed by using GROMACS with periodic boundary conditions and a 20 fs time step. Non-bonded interactions were cut off at 1.2 nm.

The Lennard-Jones potential was smoothly shifted to zero between 0.9 nm and the cutoff distance by using a third degree polynomial function. The neighbor list was updated every 10 steps using a 1.4 nm cutoff. Particle mesh Ewald (PME) was applied for long-range electrostatics.

In comparison to all-atom models, the dynamics observed with CG models is faster. The main reason is that the underlying energy landscape is much smoother as a result of the larger particle sizes. Coarse-grained lipid lateral diffusion rates are observed to be in good agreement with experimental measurements using effective time (15). Effective time can be calculated by multiplying the simulation time by 4. The times reported in the paper are effective times.

Calculation of radial distribution. The plane of the bilayer was segmented into concentric cylinders (main text Fig. 3*A*, SI Appendix-Fig. S8). The rotational axes of the cylinders coincided with the rotational axis of the TBM. The numbers of DLPC and DPPC molecules were counted in each segment of radius r and averaged over 80 ns. The reported mol% was calculated for each segment by using: $DLPC\% = 100 \times N_{DLPC} / \left(N_{DLPC} + N_{DPPC} \right)$.

REFERENCES

1. Gu L-Q*, et al.* (2000) Reversal of charge selectivity in transmembrane protein pores by using non-covalent molecular adapters. *Proc.Natl.Acad.Sci.USA* 97:3959-3964.

2. Gu L-Q, Cheley S, & Bayley H (2001) Prolonged residence time of a noncovalent molecular adapter, b-cyclodextrin, within the lumen of mutant a-hemolysin pores. *J.Gen.Physiol.* 118:481-494.

3. Howorka S & Bayley H (1998) Improved protocol for high-throughput cysteine scanning mutagenesis. *Biotechniques* 25:766-772.

4. Cheley S, Braha O, Lu X, Conlan S, & Bayley H (1999) A functional protein pore with a "retro" transmembrane domain. *Protein Sci.* 8:1257-1267.

5. Cheley S*, et al.* (1997) Spontaneous oligomerization of a staphylococcal a-hemolysin conformationally constrained by removal of residues that form the transmembrane b barrel. *Protein Eng.* 10:1433-1443.

6. Montal M & Mueller P (1972) Formation of bimolecular membranes from lipid monolayers and study of their electrical properties. *Proc.Natl.Acad.Sci.USA* 69:3561-3566.

7. Hwang WL, Chen M, Cronin B, Holden MA, & Bayley H (2008) Asymmetric droplet interface bilayers. *J Am Chem Soc* 130:5878-5879.

8. Bayley H*, et al.* (2008) Droplet interface bilayers. *Mol. BioSystems* 4:1191-1208.

9. Song L*, et al.* (1996) Structure of staphylococcal a-hemolysin, a heptameric transmembrane pore. *Science* 274:1859-1865.

10. Šali A, Potterton L, Yuan F, van Vlijmen H, & Karplus M (1995) Evaluation of comparative protein modeling by MODELLER. *Proteins: Structure, Function, and Bioinformatics* 23(3):318-326.

11. Bond PJ & Sansom MSP (2006) Insertion and Assembly of Membrane Proteins via Simulation. *J Am Chem Soc* 128(8):2697-2704.

12. Van Der Spoel D*, et al.* (2005) GROMACS: fast, flexible, and free. *J Comput Chem* 26(16):1701-1718.

13. Berendsen HJC, Postma JPM, van Gunsteren WF, DiNola A, & Haak JR (1984) Molecular dynamics with coupling to an external bath. *J Chem Phys* 81(8):3684-3690.

14. Monticelli L*, et al.* (2008) The MARTINI coarse grained force field: extension to proteins. *J. Chem. Theory and Comput.* 4:819-834.

15. Marrink SJ, de Vries AH, & Mark AE (2003) Coarse Grained Model for Semiquantitative Lipid Simulations. *J Phys Chem B* 108(2):750-760.

16. Kučerka N, Nieh M-P, & Katsaras J (2011) Fluid phase lipid areas and bilayer thicknesses of commonly used phosphatidylcholines as a function of temperature. *Biochimica et Biophysica Acta (BBA) - Biomembranes* 1808(11):2761-2771.

17. Wu Y, He K, Ludtke SJ, & Huang HW (1995) X-ray diffraction study of lipid bilayer membranes interacting with amphiphilic helical peptides: diphytanoyl phosphatidylcholine with alamethicin at low concentrations. *Biophys J* 68(6):2361-2369.

18. Shinoda K, Shinoda W, Baba T, & Mikami M (2004) Comparative molecular dynamics study of ether- and ester-linked phospholipid bilayers. *J Chem Phys* 121(19):9648-9654.

19. Tristram-Nagle S*, et al.* (2010) Structure and water permeability of fully hydrated diphytanoylPC. *Chem Phys Lipids* 163(6):630-637.

Table S1. Characteristic thickness values of a DPhPC bilayer (16-19).

Method	Bilayer thickness (Å)[a]	Hydrocarbon region thickness (Å)	Reference
Simultaneous small-angle neutron and X-ray scattering	36.3 ± 0.7	27.8 ± 0.6	16
X-ray lamellar diffraction	38.0	--	17
Molecular Dynamics	37.1 ± 0.4	28.0 ± 3.3	18
Neutron and X-ray scattering	36.4	27.2	19

[a] distance between phosphate headgroups

	Length (Å)	$I_o^{+160\ mV}$ (pA)	Noise[a]
NN	93.0 ± 2.2	166.1 ± 6.8	0.5 ± 0.1
Δ2	89.2 ± 0.9	188.2 ± 6.6	0.9 ± 0.3
Δ4	82.4 ± 1.3	195.2 ± 8.3	3.5 ± 0.3
Δ6	77.0 ± 0.9	163.0 ± 3.9	3.7 ± 0.7
Δ8	71.9 ± 0.8	160.2 ± 6.8	2.4 ± 0.4

[a] $\text{Noise} = \sqrt{(\sigma^{+160mV})^2 + (\sigma^{+0mV})^2}$

Table S2. The open pore current levels and noise values for the TBM proteins. Single-channel recordings were carried out at +160 mV (*trans* compartment positive, relative to *cis* at ground) and at 0 mV (n ≥ 3 experiments). Gaussian fits were applied to current histograms obtained at +160 mV. The peak value was the mean open pore current (I_O, ± standard deviation). The mean noise values (± s.d.)[a] were obtained from 3 or more experiments. The current amplitude was determined from 500 ms of a recording and the rms noise from 1000 ms of a recording. The numbers of experiments (n) were: TBMΔ2, 3; TBMΔ4, 3; TBMΔ6, 6; TBMΔ8, 6. The current signals were filtered at 1 kHz and acquired at 5 kHz.

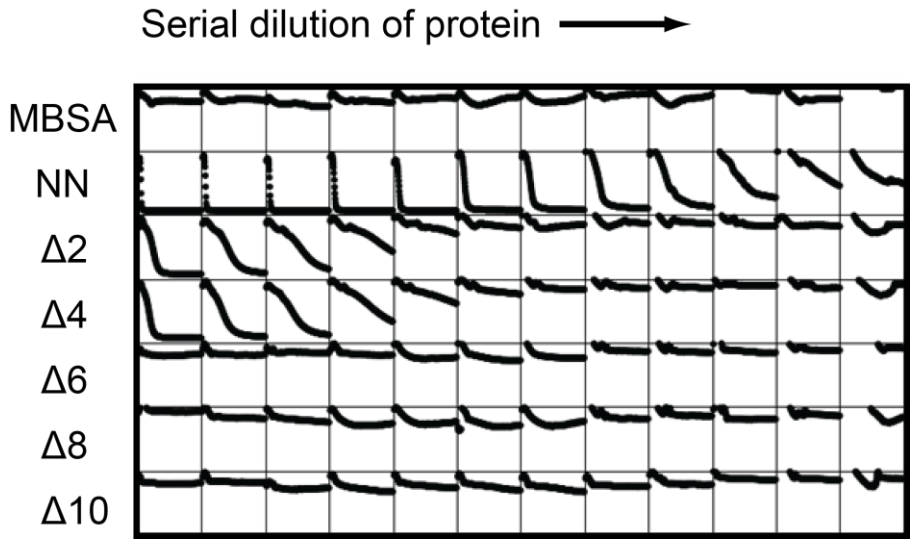

Fig. S1. Hemolytic activity of the αHL and TBM proteins. Freshly translated protein (5 μL IVTT) was added to the first column of a 96-well plate and serially two-fold diluted across the row to give a final volume of 50 μL. More fully, 5 μL of protein was added to 95 μL of MBSA in the first column. 50 μL of MBSA was placed in each of the next ten columns, leaving the final well empty. 50 μL of the diluted protein from the first column was removed and mixed with the 50 μL of MBSA in the second column. 50 μL of diluted protein from second column was then removed and mixed with 50 μL of MBSA in the third column and so forth, until each column contained serially diluted protein. Washed rRBC (50 μL, ~1% in MBSA) was added to each well to give a final volume of 100 μL. Lysis was recorded by monitoring the decrease in light scattered at 595 nm with a microplate reader (Bio-Rad Laboratories Ltd, UK).

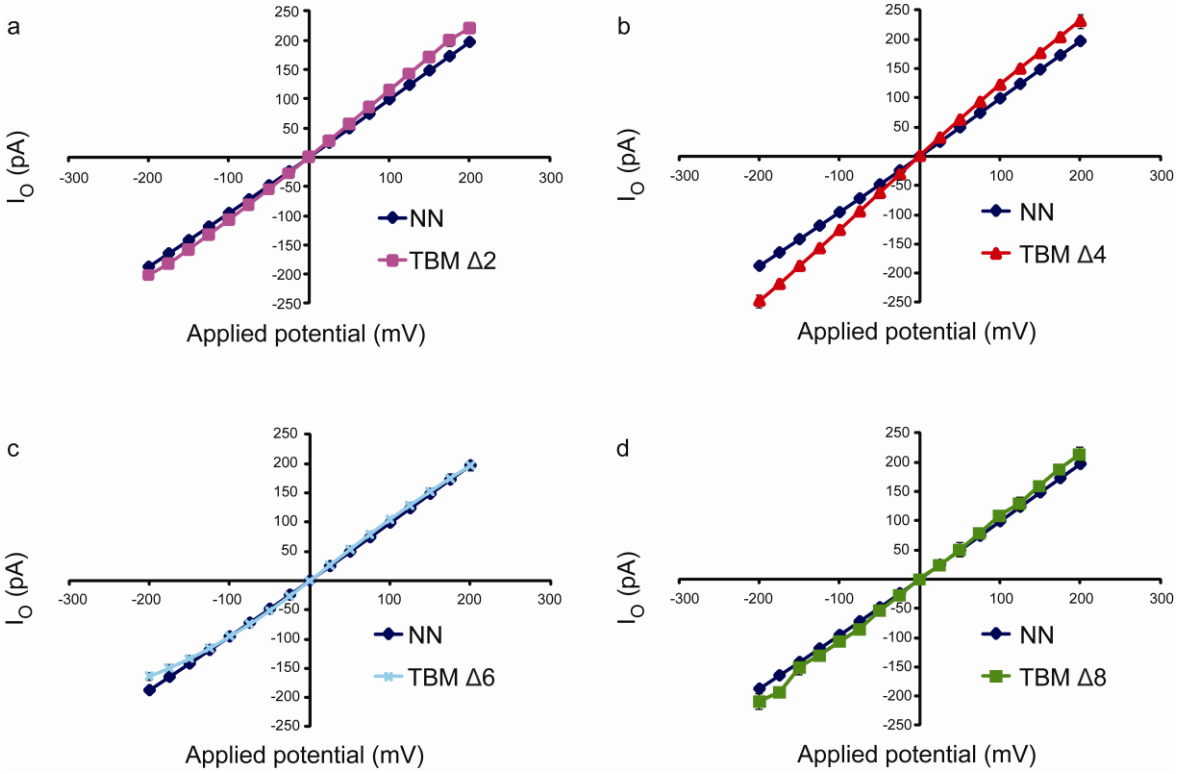

Fig. S2. Current-voltage (IV) curves for αHL NN, TBMΔ2, TBMΔ4 TBMΔ6 and TBMΔ8 pores. The mean current levels for individual pores (± s.d.) were determined (n ≥ 3) in 1 M KCl, 25 mM Tris.HCl, pH 8.0, containing 0.1 mM EDTA, over a range of applied potentials: αHL NN (navy); (*A*) TBMΔ2 (purple); (*B*) TBMΔ4 (red); (*C*) TBMΔ6 (light blue); (*D*) TBMΔ8 (green).

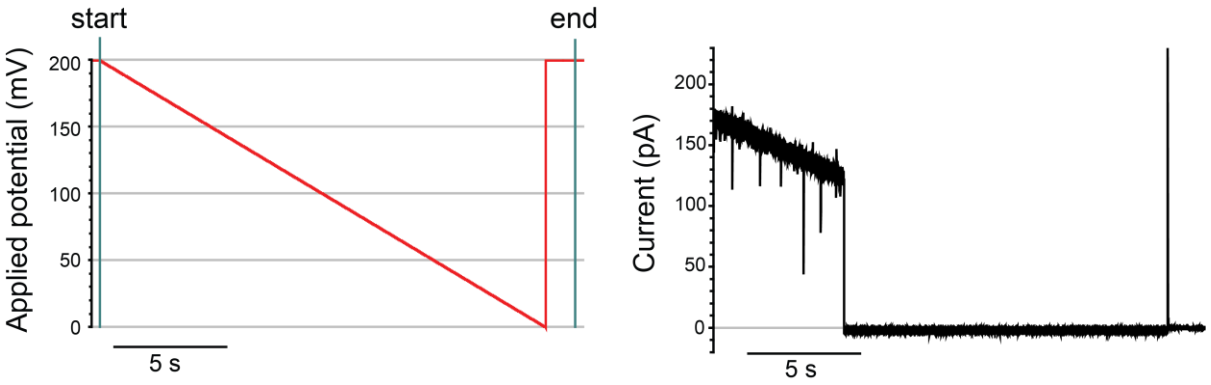

Fig. S3. Current characteristics of the TBMΔ8 pore in a voltage ramp. A TBMΔ8 pore was examined in a bilayer comprising 90% DPhPC/ 10% DLPC (w/w). A voltage ramp from +200 mV to 0 mV was applied at -10 mV s^{-1}. The pore closed at +125 mV. TBMΔ8 pores typically closed at below +100 mV.

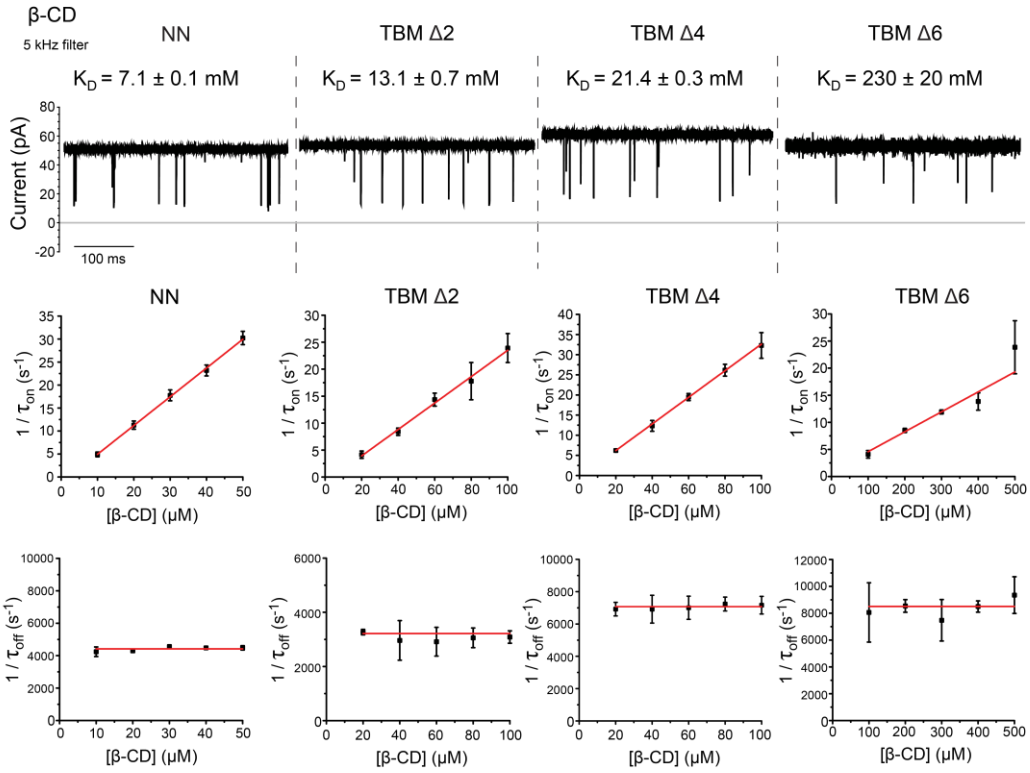

Fig. S4. β-Cyclodextrin binding to the αHL NN, TBMΔ2, TBMΔ4 and TBMΔ6 pores. *Upper,* Representative single-channel traces showing transient blockades by β-cyclodextrin (βCD). For presentation purposes, the traces were filtered (post acquisition) at 5 kHz, by using a 4-pole Bessel filter. Mean τ_{on} (inter-event intervals) and τ_{off} (βCD residence times) values (± s.d., n ≥ 3) were obtained for each αHL pore at various βCD concentrations, [βCD]. *Lower,* The association and dissociation rate constants, k_{on} and k_{off}, were determined from plots of $1/\tau_{on}$ and $1/\tau_{off}$ versus [βCD] using linear fit tools in OriginPro8. Dissociation constants ($K_D = k_{off}/k_{on}$) were calculated from the rate constants and errors (s.d.) propagated from the errors in k_{on} and k_{off} (Equation 1).

Equation 1.
$$Z = X / Y$$
$$\Delta Z = Z\sqrt{(\Delta X / X)^2 + (\Delta Y / Y)^2}$$

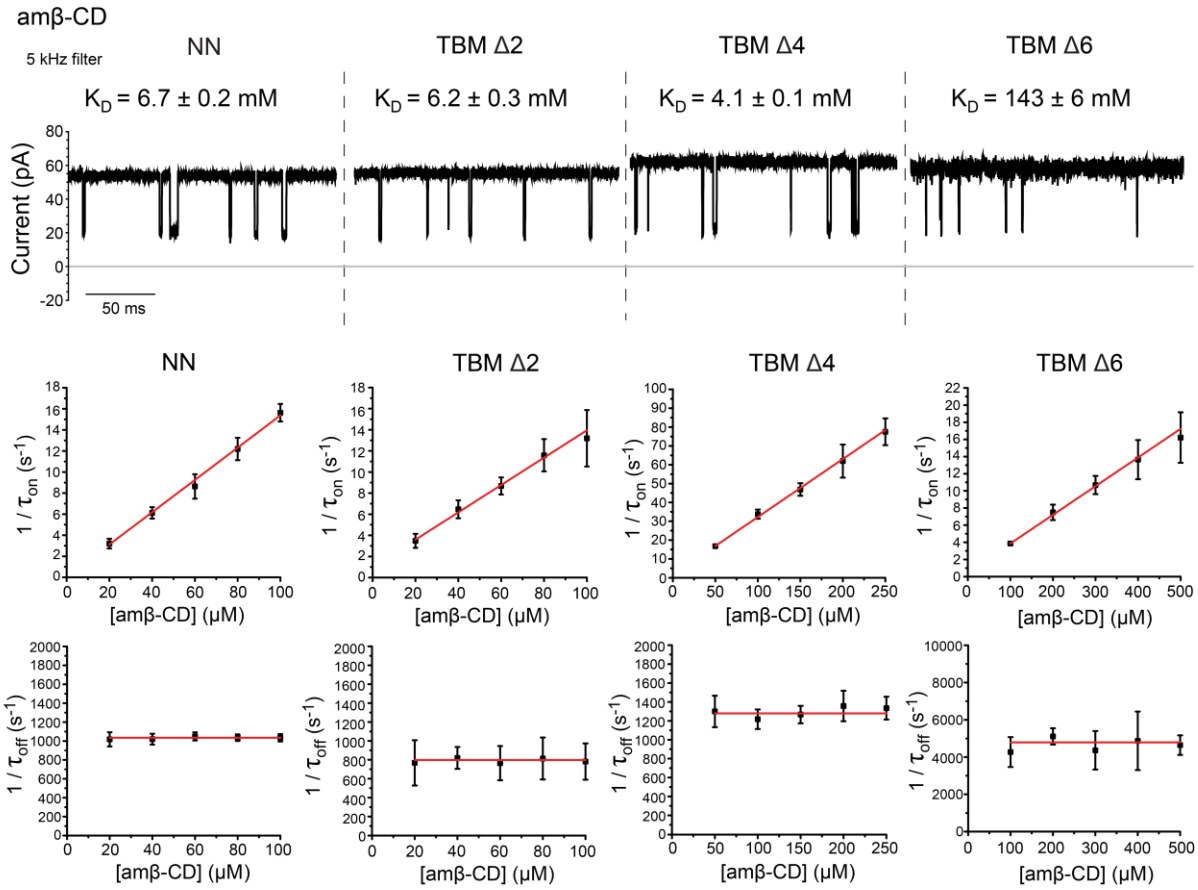

Fig. S5. Heptakis-(6-deoxy-6-amino)-β-cyclodextrin ($am_7\beta CD$) binding to the αHL NN, TBMΔ2, TBMΔ4 and TBMΔ6 pores. *Upper,* Representative single-channel traces showing transient blockades by $am_7\beta CD$. For presentation purposes, the traces were filtered (post acquisition) at 5 kHz, by using a 4-pole Bessel filter. Mean τ_{on} (inter-event intervals) and τ_{off} ($am_7\beta CD$ residence times) values (± s.d., n ≥ 3) were obtained for each αHL pore at various $am_7\beta CD$ concentrations, [$am_7\beta CD$]. *Lower,* The association and dissociation rate constants, k_{on} and k_{off}, were determined from plots of $1/\tau_{on}$ and $1/\tau_{off}$ versus [$am_7\beta CD$] using linear fit tools in OriginPro8. Dissociation constants ($K_D = k_{off}/k_{on}$) were calculated from the rate constants and errors (s.d.) propagated from the errors in k_{on} and k_{off} (Equation 1, SI Appendix-Fig. S4).

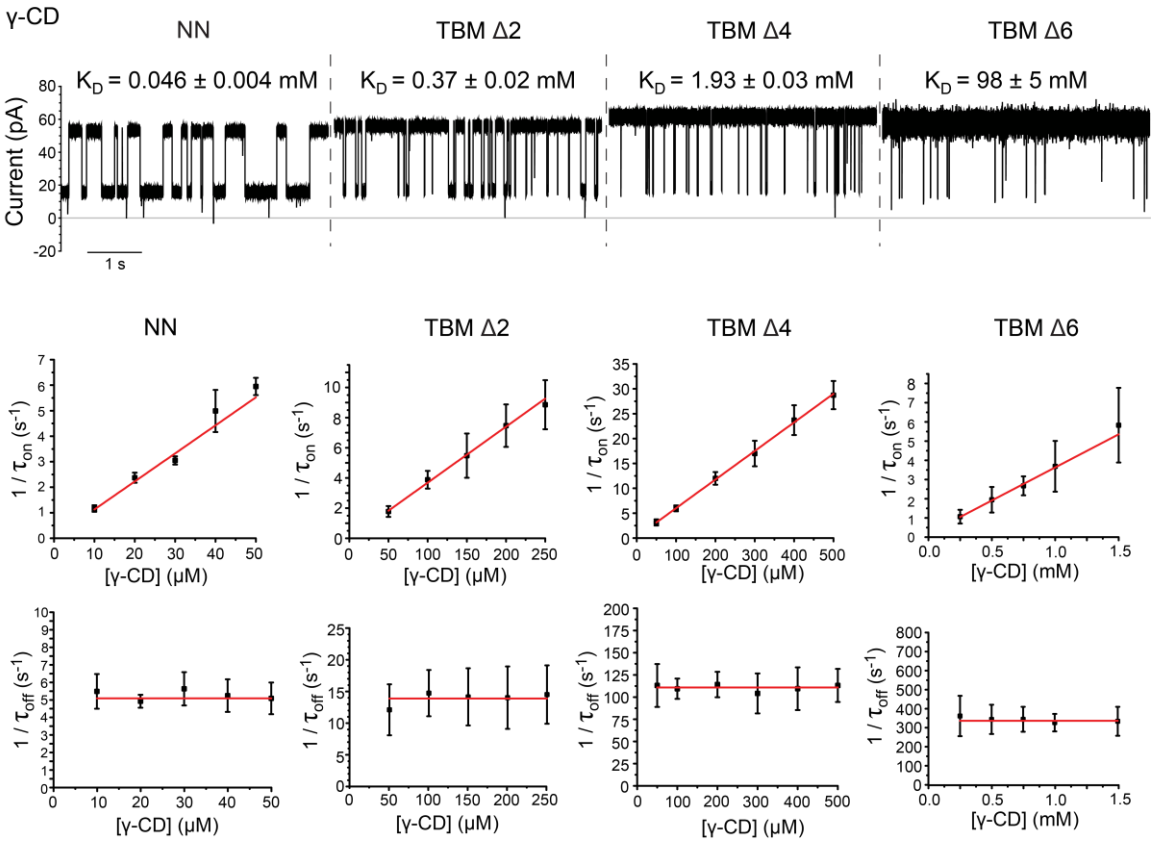

Fig. S6. γ-Cyclodextrin (γCD) binding to the αHL NN, TBMΔ2, TBMΔ4 and TBMΔ6 pores. *Upper,* Representative single-channel traces showing transient blockades by γCD. For presentation purposes, the traces were filtered (post acquisition) at 5 kHz, by using a 4-pole Bessel filter. Mean τ_{on} (inter-event intervals) and τ_{off} (γCD residence times) values (± s.d., n ≥ 3) were obtained for each αHL pore at various γCD concentrations, [γCD]. *Lower,* The association and dissociation rate constants, k_{on} and k_{off}, were determined from plots of $1/\tau_{on}$ and $1/\tau_{off}$ versus [γCD] using linear fit tools in OriginPro8. Dissociation constants ($K_D = k_{off}/k_{on}$) were calculated from the rate constants and errors (s.d.) propagated from the errors in k_{on} and k_{off} (Equation 1, SI Appendix-Fig. S4).

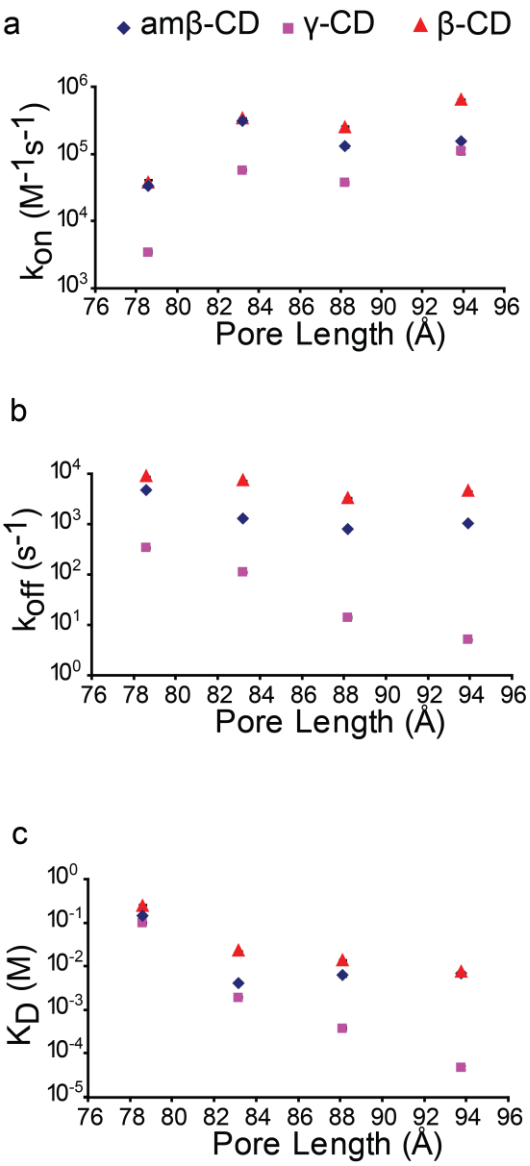

Fig. S7. Kinetic constants for cyclodextrins with the αHL NN, TBMΔ2, TBMΔ4 and TBMΔ6 pores. (*A*) Association rate constants, k_{on}, for the cyclodextrins βCD, am_7βCD and γCD plotted against pore length (TBMΔ6, TBMΔ4, TBMΔ2 and αHL NN, left to right). (*B*) Dissociation rate constants, k_{off}, for the cyclodextrins βCD, am_7βCD and γCD plotted against pore length. (*C*) Equilibrium dissociation constants, $K_D = k_{off}/ k_{on}$, for the cyclodextrins βCD, am_7βCD and γCD plotted against pore length. Error bars are smaller than the symbols in most cases.

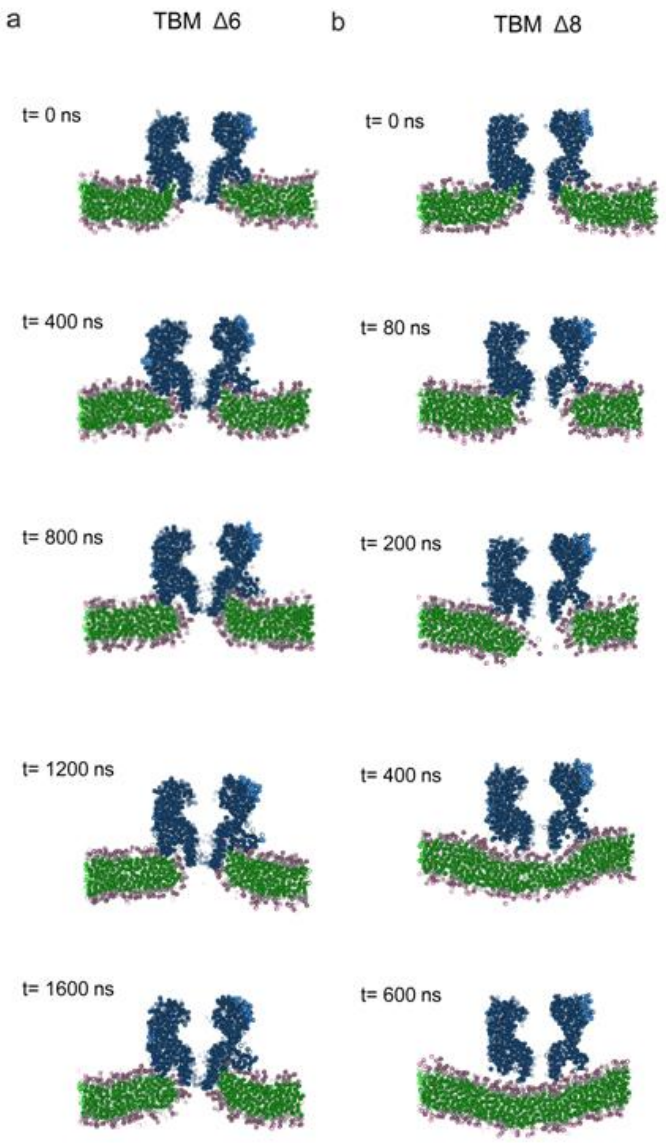

Fig. S8. MD simulations. Molecular dynamics simulations of the behavior of truncated αHL pores in bilayers of 90 mol% DPPC and 10 mol% DLPC: (*A*) TBMΔ6; (*B*) TBMΔ8. Snapshots at various time points during simulations are shown. Each simulation contained a bilayer with a lateral area of ~300 nm^2, and only a portion is shown in the snapshots. TBMΔ6 and TBMΔ8, blue spheres; lipid headgroups, pink spheres; hydrocarbon side-chains, green, respectively. Water and ions are omitted for clarity.

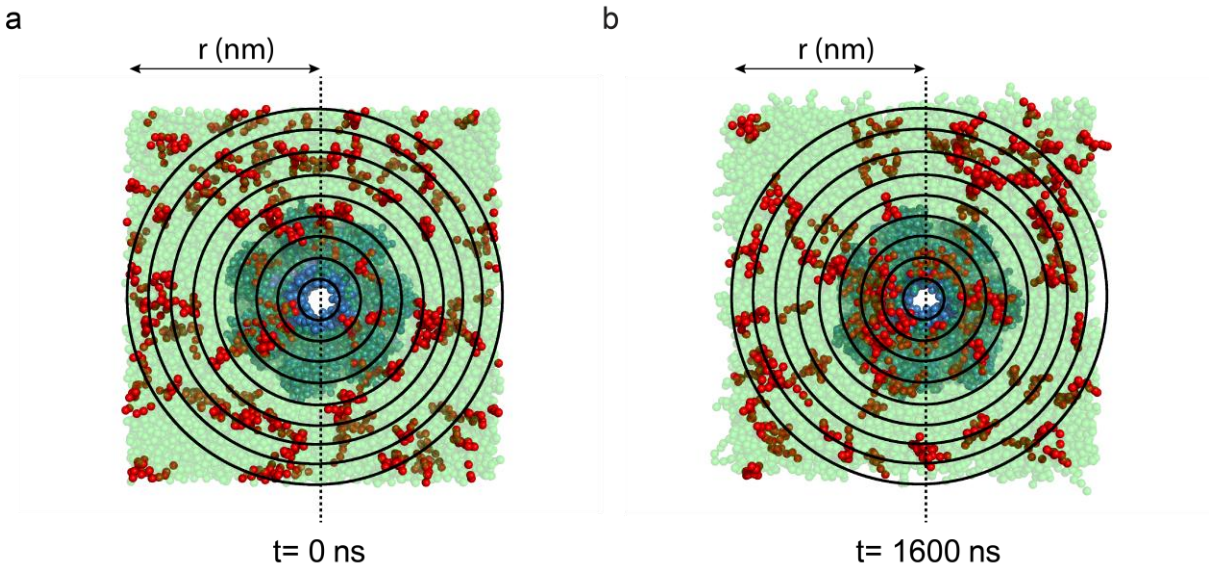

Fig. S9. Mapping of lipid distributions during MD simulation. Bottom view snapshots of TBMΔ6 in bilayers of 90 mol% DPPC and 10 mol% DLPC: (*A*) 0 ns; (*B*) 1600 ns. DLPC and DPPC molecules are shown as red and green spheres, respectively. The DLPC molecules move into proximity with the pore. The data from such simulations are plotted in Fig. 3*A* in the main text.

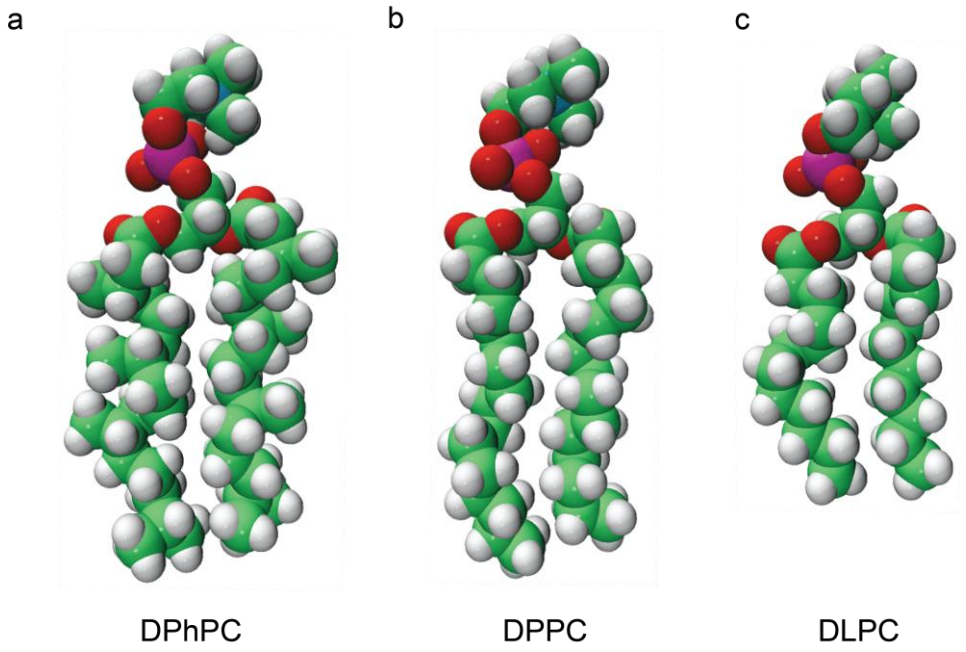

Fig. S10. Chemical structures of lipids. (*A*) DPhPC (1,2-diphytanoyl-*sn*-glycero-3-phosphocholine); (*B*) DPPC (1,2-dipalmitoyl-*sn*-glycero-3-phosphocholine); (*C*) DLPC (1,2-dilauroyl-*sn*-glycero-3-phosphocholine). The structures were produced with ChemBioDraw Ultra 12.0.

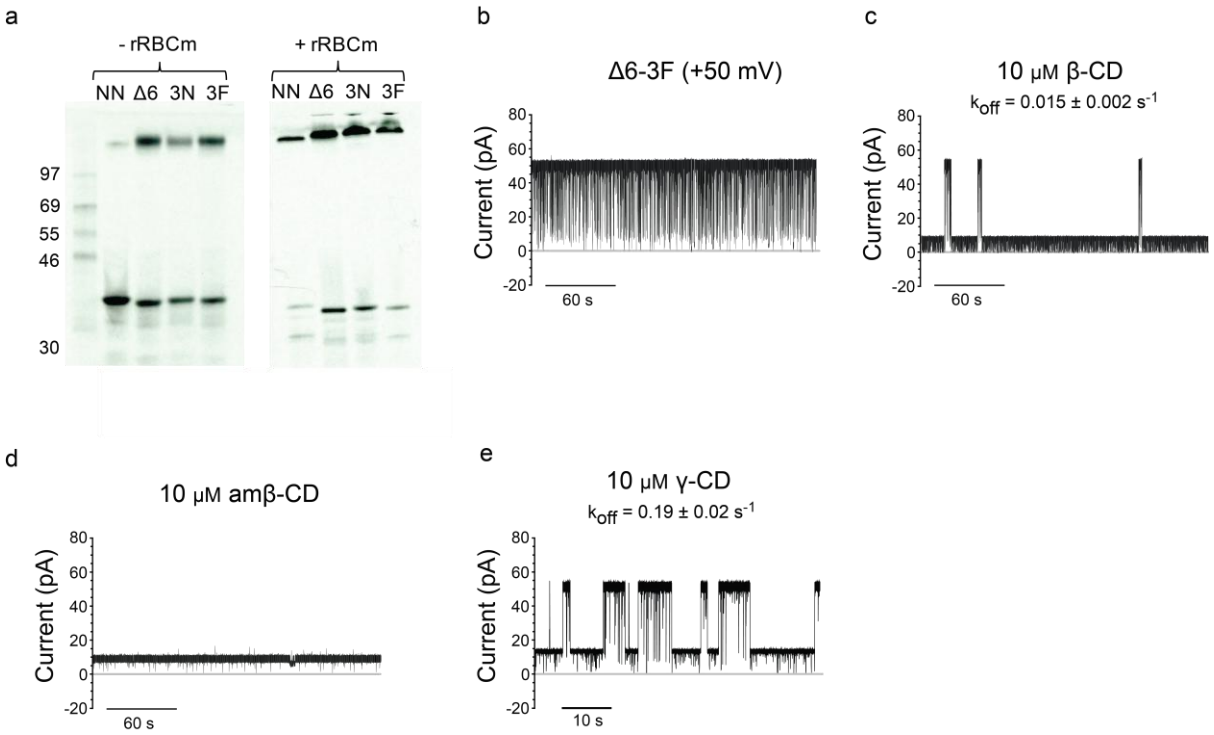

Fig. S11. Properties of TBMΔ6/M113F. (*A*) SDS-PAGE analysis of TBMΔ6/M113F after expression by IVTT in the absence (-rRBCm) and presence (+rRBCm) of rabbit red blood cell membranes (rRBCm). NN: full-length E111N/K147N; Δ6, TBMΔ6; 6N: TBMΔ6/M113N and 6F: TBMΔ6/M113F. (*B*) Representative single-channel trace of TBMΔ6 in the open state. (*C, D, E*) Current blockades in the presence of 10 μM βCD, 10 μM am_7βCD and 10 μM γCD, respectively. Recordings were made in 1 M KCl, 25 mM Tris.HCl, 0.1 mM EDTA, pH 8.0, at +50 mV. The dissociation rate constants, k_{off}, were determined from mean values of $1/\tau_{off}$.